43rd Turbomachinery & 30th Pump Users Symposia (Pump & Turbo 2014)
September 23-25, 2014 | Houston, TX | pumpturbo.tamu.edu

A LATERAL ROTORDYNAMICS PRIMER ON ELECTRIC SUBMERSIBLE PUMPS (ESPs) FOR DEEP SUBSEA APPLICATIONS

Dr. Dara W. Childs
Leland T. Jordan Professor
Turbomachinery Laboratory
Texas A&M University
College Station, TX, USA

Clay S. Norrbin
Graduate Research Assistant
Turbomachinery Laboratory
Texas A&M University
College Station, TX, USA

Stephen Phillips
Senior Research Associate
Turbomachinery Laboratory
Texas A&M University
College Station, TX, USA

Dr. Childs is the Leland T. Jordan Chair of Mechanical Engineering and has been director of The Turbomachinery Laboratory since 1984. He conducts research related to fluid-structure forces in rotordynamics. He teaches undergraduate and graduate courses in Dynamics and a graduate course in Rotordynamics.

Clay Norrbin is currently a PhD candidate at Texas A&M University. He works under the direction of Dr. Dara W. Childs on improving the life of electrical submersible pumps through rotordynamic analysis. Mr. Norrbin received his Bachelors of Science in Mechanical Engineering from Florida State University.

Stephen Phillips is a Senior Research Associate at the Turbomachinery Laboratory (TL) at Texas A&M University, in College Station, Texas. He has 20 years of experience conducting testing and measurements of rotating machinery seals and bearings for dynamic parameter identification. Mr. Phillips utilizes and develops the latest fluid-film bearing/seal codes and lateral/torsional rotordynamics tools (XLTRC^2). In unison with employing FEA, solid modeling, and simulation, his primary duties include supervision of design, modeling, specification, assembly, and operation of various fluid-flow/structure interaction test facilities. Mr. Phillips directed operations of the Houston & Middle East Turbomachinery Symposia and the Pump Symposium for seven years. He has co-authored many papers and participated in numerous short courses and symposia venues on rotating machinery.
Mr. Phillips holds a B.S. in Mechanical Engineering from Texas A&M University (1993) and is a member of ASME.

ABSTRACT

Stability and synchronous-response predictions are presented from a rotordynamic analysis for a 20-stage *pump segment* of an Electrical Submersible Pump (ESP) assembly. A two-line rotor-housing model is used to model the pump's rotor and its housing. The model dimensions are based on direct measurements of an ESP. The pump and housing are only connected together at each stage by reaction forces from seals and bushings. The rotor model is pinned to the housing at the rotor's ends. The housing model is pinned to ground. At separate times during a field's lifetime, an ESP in deep subsea operation will handle: (1) a low-viscosity fluid comparable to water, and (2) a high-viscosity fluid that is representative of oil-water emulsions. Calculations were performed for the extremes of density and viscosity.

Synchronous response predictions are presented for: (1) relative rotor-housing motion, and (2) housing velocity-response amplitudes. The synchronous response was driven by mechanical imbalance (4W/N API balance spec), hydraulic imbalance (midrange of expected levels for an investment-cast impeller), and bent-shaft excitation (based on representative data from direct bent-shaft eccentricity measurements). The predicted response amplitudes were comparable for the hydraulic and mechanical imbalances, and much larger for the bent-shaft excitation.

When handling water, the rotor-housing model is predicted to be stable at new (centered) 1X clearances but rapidly becomes unstable with enlarged clearances (2X, 3X), primarily due to rapidly dropping rotor-housing natural frequencies. These instabilities arise due to fluid rotation in the annular seals/bushings/bearings of pump stages. They are not related to "oil-whirl" in a rotor supported largely by fluid-film bearings. Introducing effective swirl brakes for the stages' wear ring seals was investigated for a pump running at 3600 rpm. Their predicted impact on stability and synchronous response were: (1) Onset speeds of instabilities (OSIs) were elevated well above running speed, and (2) Synchronous response amplitudes were reduced modestly. Housing-response amplitudes varied considerably with the choice of housing-termination locations.

For a pump rotor length of L_r and centered housing of lengths ($1.5L_r$, $2L_r$, and $3L_r$), a resonance peak moves across 3600 rpm. Large housing vibration amplitudes associated with resonance were predicted (at some axial locations) that would exceed most vibration codes; however, relative rotor-stator-response amplitudes were a small fraction of clearances for all cases.

When handling emulsions at markedly higher viscosities, with a pump speed of 3600 rpm, the rotor-housing model was unstable for seals *with new clearances at a centered position*, the predicted OSI was below 300 rpm. The OSI rapidly increased as the seals were displaced eccentrically, quickly elevating the rotor-stator natural frequencies above 1800 rpm and the OSI above 3600 rpm. Only a modest relative eccentricity (0.1~0.2) was required to assure stability. With a stable model due to eccentrically displaced seals, the synchronous relative rotor-housing-motion amplitudes were a small fraction of seal clearances. As with water applications, the housing motion continued to show a sharp peak near running speed.

An ESP housing can contact the column piping in many possible scenarios (axial locations, contact-area length or girth, etc.). A mid-span, point radial contact was examined and modeled as a stiff-spring connection from the housing to ground. For both water and oil-water emulsions, a stiff housing-to-column contact produced major elliptical housing motion (versus circular motion without contact). However, it had a comparably minor impact on relative rotor-housing response amplitudes or rotordynamic stability.

Based on horizontal, surface ESP applications, Durham in 1990 stated that most ESP failures were initiated by mechanical-seal failures, and the mechanical-seal failures were caused by lateral vibrations. The pump sections of the assemblies were not failing. The first lesson from the present study is that a *full-assembly* model will be needed (versus the pump-section-only model studied here) to directly consider the impact of pump vibrations on ESP mechanical seal failures. The full-assembly's model stability is of interest versus a pump-only model. Also, housing vibration levels that are immediately adjacent to the mechanical seal locations need to be predicted.

In conventional horizontal pumps, unstable subsynchronous-response levels can be much higher than synchronous response. Hence, rotordynamic instabilities may be a substantially greater hazard than synchronous-response amplitudes in causing ESP mechanical-seal failures. However, ESPs have many coupled rotor-housing modes that could be excited by either instabilities or synchronous response, and large synchronous-housing motion near mechanical seals could also create large and damaging seal vibration levels.

Briefly, other lessons are:

1. A straightforward rotordynamic model for an ESP produces predictions that agree well with the limited existing ESP vibration test data.
2. Instabilities for ESPs handling low-viscosity fluids can be prevented by using conventional swirl brakes.
3. Instabilities for ESPs that are handling high-viscosity fluids (with new clearances) can be managed by operating plain annular seals at comparatively low static eccentric ratios (0.1~0.2). Swirl brakes are not effective with new clearances.
4. For ESPs handling high-viscosity fluids with enlarged clearances (2X, 3X), increasing static eccentricity ratios is not effective in elevating OSIs.
5. For ESPs handling high-viscosity fluids with enlarged clearances (2X, 3X), swirl brakes are effective in elevating OSIs.

Predictions of this study support the following views and recommendations: (1) Applying swirl brakes to ESP wearing-ring seals can significantly increase ESP lifetimes, (2) Models and analysis of a full ESP assembly are needed to directly examine options for reducing vibration levels at mechanical seals, thereby extending ESP lifetimes, and (3) Analyses, models, and tests are needed to quantify Durham's views regarding the failure of mechanical seals due to lateral vibrations.

INTRODUCTION

ESPs are down-hole pumps that have been used in large numbers for many years in the production of oil for surface fields. They have been manufactured and designed as a commodity product that could be produced at low prices and quickly replaced if problems arise. They are now being seriously considered for use in deep subsea applications where reliability is a premium. Specifically, oil companies hope to a obtain seven-year lifetimes in deep subsea wells. In 2012, one OEM manufacturer projected two-year lifetimes [1] for upgraded ESPs.

The historical problems with ESPs and their vibration characteristics is that they are not accessible for instrumentation. In 1990, Durham et al. [2] looked at vibration characteristics of ESPs in accessible, surface, *horizontal* applications. (In the authors' opinion, this is the best paper that has been published on ESP vibrations and their impact on ESP lifetimes.) Durham's abstract reads as follows:

> *Electric submersible pumps* (*ESPs*) *historically have had short run lives. Their failures usually were unexplained and accepted as the norm. Because the equipment has generally been downhole, finding all the influences that shorten equipment life expectancy has been difficult. Horizontal surface installations for water injection have been made where machine operating conditions could be monitored and equipment performance analyzed.*
> *Unbalanced pump vibration has been identified as the cause of many seal problems and ultimately motor and pump failures. In fact, excessive vibration appears to be an inherent mechanical characteristic of ESPs. To illustrate the severity of this problem, this paper presents data gathered from field installations with monitoring equipment, from equipment tear-down analysis, and from statistics on ESP failure modes.*

Durham's pumps were in water-injection service and were instrumented crudely. He states, "The vibration amplitude and frequency were measured for the motor shaft with a

mechanical analyzer and a connected shaft stick. The amplitude of vibration was no greater than 0.25 mil [0.06 μm] for any of the motors. Because this is well within the acceptable vibration tolerances, we concluded that the motors were not the source of vibration."

Durham's pump's motors ran on rolling-element bearings. Typically, ESP motors operate on plain journal bearings that are subject to classic problems of *Oil Whirl*. For surface applications, oil whirl is most frequently seen in vertical pumps where the bearings are unloaded (or lightly loaded). Its motion is characterized by subsynchronous precessional response whose frequency "tracks" at a little less than 50% of running speed. Limit-cycle orbits associated with oil whirl can be as large as or frequently larger than synchronous response orbits. Large oil-whirl amplitudes can produce destructive rubbing at the bearings that definitely limits life times of vertical-pumps [3].

Figure 1 from Salas et al. [4] shows oil whirl for an ESP *motor* operating on plain journal bearings. Note that whirl *initiates at low speeds*, tracking at about 50% of running speed. Also, note that the oil-whirl subsynchronous motion response is about the same magnitude as the synchronous response.

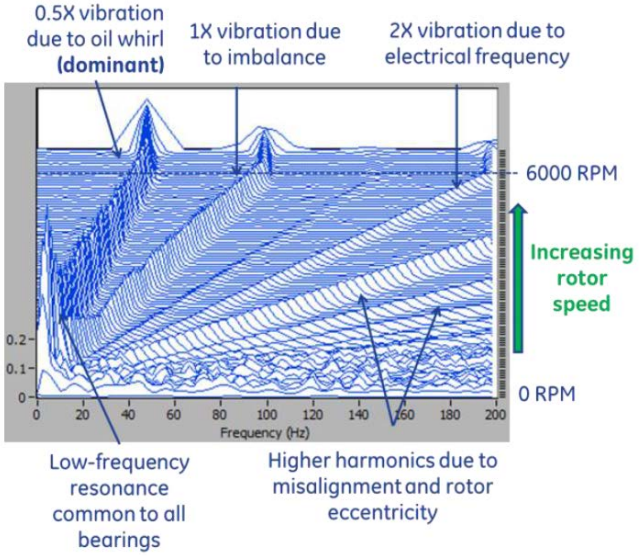

Figure 1. Oil whirl observed in an ESP electric motor, Salas et al. [4]

With increasing speeds, oil whirl can transition to *Oil Whip* at some limiting speed above which the precession frequency stops tracking at a little less than 50% of running speed and begins precessing at the pump's 1st natural frequency. Oil whirl is a nonlinear phenomenon that is not predicted by conventional linear rotordynamic models and codes. The oil-whip unstable mode and natural frequency can be identified by linear analysis; the transition from whirl to whip cannot. Salas et al. [4] observed a transition from oil whirl to oil whip.

In horizontal applications, plain journal bearings react a vertical load due to weight by: (1) developing a positive pressure sector over the bearing's converging-clearance circumferential sector, and (2) developing near-zero pressure over the diverging sector where gas cavitation prevents negative pressures from arising (see Figure 2). This reaction-enabling cavitation can be suppressed by pressurizing the bearing, leading immediately to oil whirl or oil whip. In ESP pumps, operating pressures are always sufficiently high to suppress cavitation and make every annular cavity (bearing/bushing/seal) act as a potential oil-whirl or oil-whip driver.

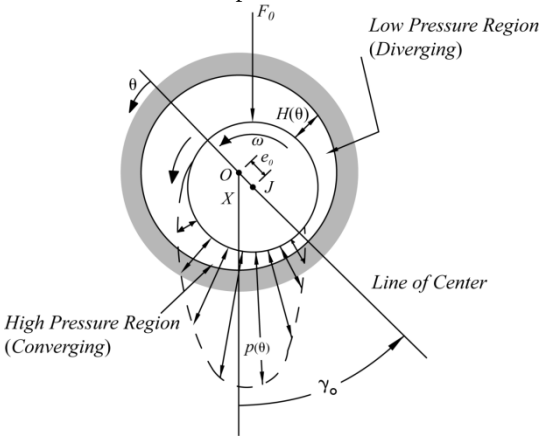

Figure 2. Plain journal bearing reacting a load through cavitation, Childs [5]

Oil Whirl is a very old problem that is remedied by replacing plain journal bearings with alternative journal bearing designs that can develop a centering force without cavitation. In 1972, Gunter [6] recommended pressure-dam bearings or other fixed-arc bearings (e.g., 3-lobe bearings with preloaded pads) as a means to develop good centering forces that would eliminate oil whirl. In 2010, Leader [7] solved an oil-whirl/oil-whip problem in a vertical sulfur pump by replacing two plain bushings with 100%-offset, 3-lobe designs. In 2002, Corbo et al. [3] replaced five shaft bushings with tilted-pad bearings in a vertical water pump that was operating in a nuclear power plant.

ESP *motor* bearings are provided with nominally clean conventional lubricants. Hence, any of these previously-employed, plain-journal-bearing replacements should readily eliminate oil whip or oil whirl in ESP motors. As noted above, in 2013, Salas et al. [4] presented a case study regarding an ESP motor that displayed subsynchronous motion in either a vertical or horizontal position. The motion displayed oil whirl at start up and proceeded in some cases to oil whip as speed was advanced. The problem was entirely eliminated when the original plain journal bearings were replaced with "high-stability" bearings of undisclosed designs.

While ESP electric motors may present continuing rotordynamic modeling challenges, their problems with oil whip and oil whirl are readily eliminated by existing technology and knowledge. That is not the case with ESP pumps, and the present paper deals with *lateral* rotordynamic issues of ESP *pumps*.

The following two classic problems exist in regard to lateral pump rotordynamics: (1) synchronous response due to imbalance when the pump is operating near a lightly damped critical speed, and (2) rotordynamic instabilities. Based on impulse excitation of a hanging pump rotor, Durham thought one of his pumps had a critical speed problem when running at 3600 rpm.

Conventional *horizontal* pumps experience instabilities that are *related* to the oil-whip instability that was resolved by Salas et al. Unstable motion arises with large, subsynchronous, precessional response at the rotor's first critical speed when the rotor is running at a higher speed. Unlike Salas' oil-whip

experience, there is no 50% "tracking" subsynchronous response from low speeds as shown in Figure 1 prior to the onset of unstable motion and no transition from whirl to whip. There can be tracking once unstable motion initiates, ranging from 70 to 80 % of running speed.

Two well-documented pump rotordynamic instabilities for horizontal pumps have been related by Massey [8] and Valantas and Bolleter [9]. Massey's pump had eleven stages and was pumping a hydrocarbon. Valantas and Bolleter's pump had five stages and was handling produced water. In both cases, unstable subsynchronous motion caused rapid wear in the pump's seals. In Massey's experience, excessive wear arising from unstable motion caused the pump to be taken off line after 100 hours. In Valantas and Bolleter's case, pumps were requiring rebuilds after thirty days; some of the wear was caused by abrasives, some by rubbing due to excessive vibrations. Figure 3 shows the very large subsynchronous motion for Valantas and Bolleter's unstable pumps. With advancing speed, the unstable motion developed suddenly at an orbital precession frequency near the pump's calculated 1st critical speed, and tracked at roughly 80% of running speed. Both pumps used a straight-through design, and both instabilities were cured by installing swirl brakes upstream of the balance-piston seal. Massey's swirl brake is shown in Figure 4. Clearly, if ESP pumps experience comparable instabilities, rapid wear and shortened lifetimes are expected.

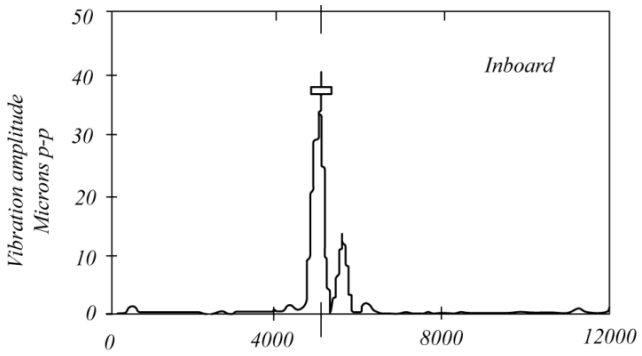

Figure 3. Synchronous (right peak) and subsynchronous (left peak) motion amplitudes versus frequency in rpm after Valantas and Bolleter [5]

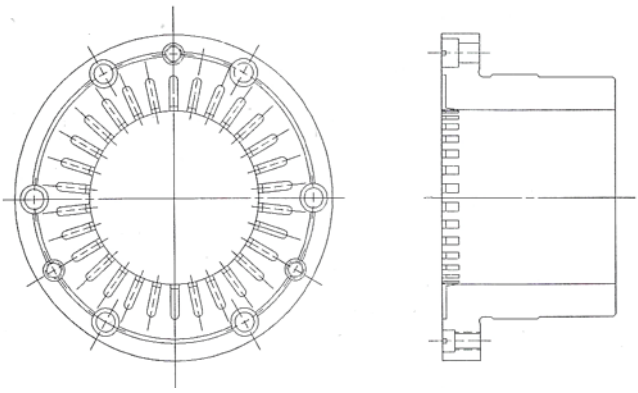

Figure 4. Swirl brake used to solve Massey's pump instability problem [8]

In 2013, Forsberg [10] presented vibration data for the ESP assembly shown in Figure 5. He densely applied accelerometers along the housing as shown in Figure 6 and presented test data for the resulting steady-state synchronous motion when operating at 3600 rpm. Ideal test data would use motion probes that provide rotor-housing relative motion; however, the data provided by Forsberg is (in the authors' opinion) the best available ESP rotordynamic data to date.

A two-line rotordynamic model (described below) is developed in this paper (rotor + housing) incorporating models for the seals and bushings that connect the rotor and housing. The pump model has 20 stages, conceptually representing one of Forsberg's pumps. Synchronous response in pumps is driven by mechanical imbalance, hydraulic imbalance, and bent-shaft excitation. The model includes all of these synchronous-excitation sources.

The rotor model does not include rotordynamic coefficients for the impellers as measured by Bolleter et al. [11] and others. Impeller stiffness and damping coefficients arise largely due to forces on the shroud, and they drop in magnitude as the clearance increases [5]. As shown in Figure 7 there is a large open space at the front of the impeller which would drastically reduce shroud reaction forces and moments. The fluid within the impellers is accounted for in the impeller's mass.

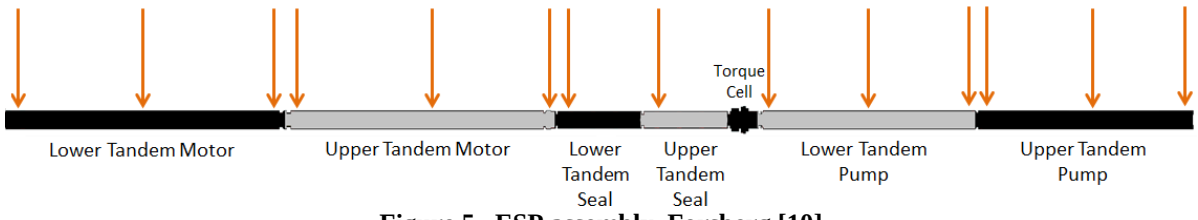

Figure 5. ESP assembly, Forsberg [10]

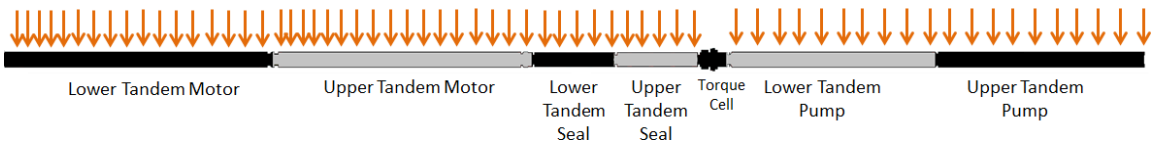

Figure 6. Axially-distributed accelerometer locations, Forsberg [10]

Any impact of the fluid between the impeller outer housing and the casing ID on Rotordynamics is neglected.

In terms of lateral ESP pump rotordynamics, analysis is performed to address the following questions:

(1) By comparison to Forsberg's results, how well does the model perform?
(2) Briefly stated, how many housing and rotor modes need to be considered?
(3) For synchronous-response vibration, what is the comparative magnitude contribution from: (a) mechanical imbalance, (b) hydraulic imbalance, and (c) bent-shaft excitation?
(4) How does uniform wear that increases seal clearances impact predicted synchronous response and stability characteristics?
(5) How does changing from water to an oil-water emulsion at much higher viscosities impact predicted synchronous response and stability?
(6) Under what conditions are ESPs predicted to be unstable?
(7) Under what conditions are swirl brakes effective in enhancing rotordynamic stability?
(8) If only a pump (rotor + housing) is modeled, how does changing the housing-model termination impact predictions?
(9) ESP housing can contact the column piping. How does a stiff local connection between the ESP housing and the well casing impact rotordynamic characteristics?
(10) What is the predicted impact of eccentric operation of seals and bushings?

ESP STAGE DESIGNS

Annular seals are well known to contribute strongly to the rotordynamic behavior of all multistage centrifugal pumps. However, most multistage pumps have clearly-defined bearings that are expected to "mainly" support the pump rotor. That is not the case with ESPs where annular seals/bushings provide virtually all of the pump rotor's lateral support.

Figure 7 presents a cross-sectional view of an ESP stage. The main flow enters the impeller at the left and proceeds through the diffuser on the right. The main leakage-flow annuli illustrated are: (1) the front wear ring seal, (2) the rear wear ring seal, (3) the interstage seal, and (4) the impeller-insert seal. The dimensions plus the expected length-to-diameter (L/D) and clearance-to-radius (C_r/R) ratios for these seals are shown in Table 1.

Table 1. Seal geometry for one stage of modeled ESP

Seal	Length (in)	Diameter (in)	New C_r (in)	C_r/R	L/D
Front Wear Ring	0.984	5.034	0.0091	0.0036	0.20
Rear Wear Ring	1.024	4.485	0.0137	0.0061	0.23
Impeller Insert	0.593	2.031	0.0156	0.015	0.29
Interstage	1.507	1.88	0.005	0.0053	0.80

These data are based on measurements from a new pump that was made available to the TAMU Turbolab. (A representative from another ESP company has stated that his company runs tighter seals with (new) radial clearances on the order of 0.0035 inch (.090 mm) at all seals, leading to reduced C_r/R values.) Each stage is assumed to produce a ΔP of 35 Psi (2.23 bars) at 3600 rpm. Table A.1 in Appendix A shows the assumed ΔP for each seal at 3600 rpm.

The impeller in Figure 7 has balancing holes, and *predictions in this paper are for stages with balance holes.* Leakage leaves the impeller and moves from right to left into the cavity at the impeller front face, then radially inwards through an axial face seal before entering the front wear ring seal. At the right-hand side of the impeller discharge, leakage flow proceeds radially inwards through an axial face seal and then from left to right through the rear wear ring seal before exiting through the balance holes.

For the main discharge flow, the diffuser creates a pressure rise before entering the next downstream stage. That pressure rise forces leakage flow back along the shaft from right to left, first through the interstage seal, and then through the impeller-insert seal. Because of the balance holes, the exit pressure at the left of the impeller-insert seal is assumed to be modestly above the impeller inlet pressure; hence, the leakage flow that leaves the impeller-insert-seal flow proceeds from right to left out through the balancing holes.

The impeller shown in Figure 8 does not use balance holes. Leakage flow through the front wear ring seal follows the same path. However, leakage exiting the impeller-insert seal proceeds radially outwards, then from right to left through the rear wearing-ring seal, and finally up the back side of the impeller to rejoin the main flow. This flow path (up the back side of the impeller) resembles the leakage path of conventional intermediate pump impellers.

The axial face seals can also act as thrust balancing devices, and their axial clearances can vary significantly. The axial clearances present the following two analysis complications: (1) The flow resistance varies with axial clearance, markedly changing the impacted annular seals' ΔP, and (2) Flow through the axial faces will act to preswirl the leakage flow entering the annular seals in the direction of shaft rotation.

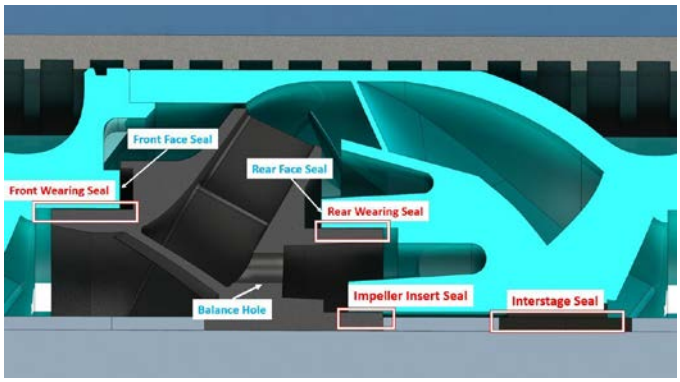

Figure 7. ESP stage with balance holes showing annular and axial seals

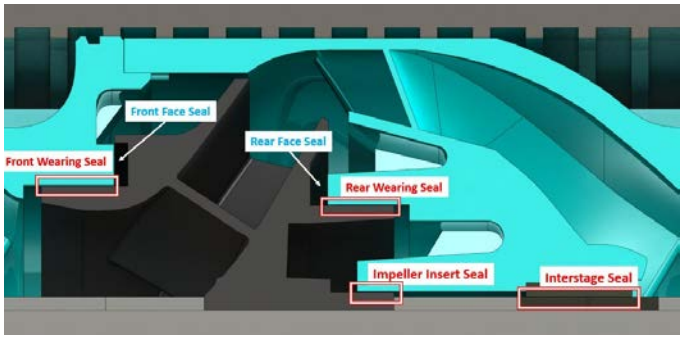

Figure 8. ESP stage without balance holes showing annular and axial seals

ESP ANNULAR-SEAL OPERATING CONDITIONS AND MODELS

For deep subsea applications, the fluid properties of the oil mixture being pumped can change dramatically. Both initially and towards the end of a field's life, the viscosity is low, approaching the viscosity of water. At some intermediate time, the pump will handle oil-water emulsions with comparatively high viscosities [12]. ESPs generally run at 1800 and 3600 rpm. At 3600 rpm, the stage ΔP is on the order of 35 psi (2.4 bars).

In the centered position, the seal's axial Reynolds number is defined by

$$R_W = \frac{\rho(2C_r)}{\mu} W_0, \tag{1}$$

where W_0 is the bulk-flow axial velocity. The circumferential Reynolds number is

$$R_\omega = \frac{\rho(C_r)}{\mu} R\omega, \tag{2}$$

where ω is the shaft's angular velocity. The vector Reynolds number is

$$R_e = \sqrt{R_W^2 + R_\omega^2} \tag{3}$$

When handling low viscosity fluids, the ΔP at 3600 rpm is large enough to produce pressure-drop-dominated turbulent flow in the seals such that centering forces are (mainly) produced via the Lomakin (1958) effect [13]. For a *centered position*, a Lomakin seal is modeled as

$$-\begin{Bmatrix} F_x \\ F_y \end{Bmatrix} = \begin{bmatrix} K & k \\ -k & K \end{bmatrix} \begin{Bmatrix} x \\ y \end{Bmatrix} + \begin{bmatrix} C & c \\ -c & C \end{bmatrix} \begin{Bmatrix} \dot{x} \\ \dot{y} \end{Bmatrix} + M \begin{Bmatrix} \ddot{x} \\ \ddot{y} \end{Bmatrix} \tag{4}$$

This eccentricity-independent model is considered to be valid for small motion about static eccentricity ratios ε_0 *out to about 0.5, where* $\varepsilon_0 = e_0 / C_r$, and e_0 *is the static seal offset.* As shown in Figure 9, the Lomakin-Effect pressure distributions create a reaction force via a trade-off in the seal pressure drop between the inlet loss and friction-factor losses along the seal's walls. Except for the dependence of ΔP on ω, the centering force due to the direct stiffness coefficient *K* is not developed directly from fluid rotation within the seal.

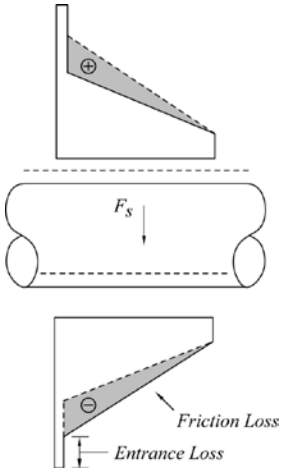

Figure 9. The Lomakin effect, Childs [4]

When handling high-viscosity emulsions, the flow is laminar and dominated by circumferential flow. In these laminar-flow conditions, the seals/bushings act more like plain, uncavitated journal bearings and are modeled by

$$-\begin{Bmatrix} f_{bx} \\ f_{by} \end{Bmatrix} = \begin{bmatrix} K_{xx} & K_{xy} \\ K_{yx} & K_{yy} \end{bmatrix} \begin{Bmatrix} \Delta x \\ \Delta y \end{Bmatrix} + \begin{bmatrix} C_{xx} & C_{xy} \\ C_{yx} & C_{yy} \end{bmatrix} \begin{Bmatrix} \Delta \dot{x} \\ \Delta \dot{y} \end{Bmatrix} + \begin{bmatrix} M_{xx} & M_{xy} \\ M_{yx} & M_{yy} \end{bmatrix} \begin{Bmatrix} \Delta \ddot{x} \\ \Delta \ddot{y} \end{Bmatrix} \tag{5}$$

The rotordynamic coefficients in this model are strong functions of ε_0.

The flow is assumed to be laminar for R_e less than 1800, turbulent for flow greater than 5000, and in the transition region between 1800 and 5000. With the oil-water emulsion and progressively increasing clearances, the flow remains laminar. With new clearances and water, the flow regime start laminar, shifts to transition, and then to fully-turbulent flow as speed and ΔP increase. Increasing the clearance will accelerate the shift to fully turbulent flow.

The reaction forces developed by plain seals and bushings arise due to a combination of Lomakin effects and fluid rotation. For motion about an eccentric position, Eq. (5) can be used to model any smooth annular seal. San Andrés 1996 bulk-flow model [14] can be used to calculate the leakage flow and appropriate rotordynamic coefficients for a smooth seal in an arbitrary position (displacement and rotation) relative to the stator for laminar, transition, and turbulent flow. With constant speed and a fixed ΔP, changing only the fluid viscosity produces predictions of significantly different static centering-force and rotordynamic behavior.

Structural Dynamics Model

Figure 10 illustrates *part* of an assembled ESP pump, showing five stages driven through the central shaft. The stages are held within an outer housing that provides almost all the structural strength; the central shaft provides minimal strength. Beam elements are used to model the housing and the shaft.

Figures 11 show a spline coupling that is used to attach one pump shaft to another pump shaft or a pump shaft to a motor shaft. A pump shaft can also terminate in a plain bushing that has no imposed ΔP. One question involved in modeling an ESP is: Where do you stop the model? The question applies to the housing and the shaft. In regard to the shaft, the pump rotor

model's ends are pinned (with respect to the housing), assuming that either the spline coupling or an end bushing provides a near rigid support. In regard to terminating the housing model, results for analyses with three different termination locations are presented below.

Figure 12 shows a cross section of the 2-line structural-dynamics model. Each impeller is assumed to be rigidly connected to the shaft and (only) connected to the housing by reaction forces from the annular seals of Figure 7. The shaft diameter is 1.5 inches (38.1mm). The housing has an ID of 9.5 inches (0.241 m), and a wall thickness of 0.375 inches (9.53mm). The seal dimensions were provided in Table 1.

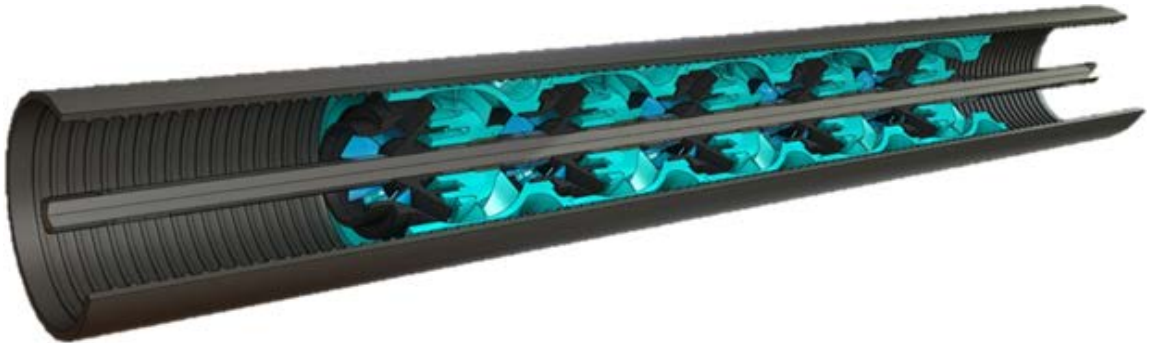

Figure 10. View showing part of an ESP pump section

Figures 11. (bottom) Female segment of spline coupling, (top) Male portion of spline coupling.

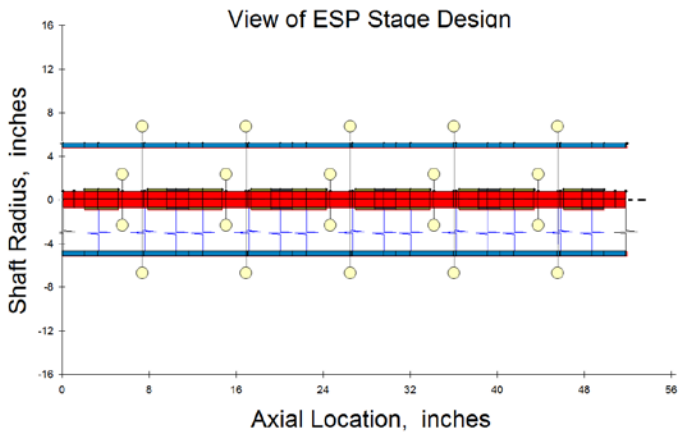

Figure 12. Model cross section

The rotor model has 320 stations with each station having four degrees of freedom (two displacements and two rotation degrees of freedom). The rotor-housing model provides station locations for each seal/bushing location plus accounting for the mass-center locations of impellers and spacer bushings. Consequently, the rotor model has 1280 degrees of freedom (DOFs).

The housing model is terminated by pinned connections to ground. Looking back at Figure 5, the housing for the full ESP assembly will customarily extend beyond the pump section. To consider the impact of various housing terminations, the following different termination locations are considered:

(a) Housing terminated at the end of the rotor section; both rotor and housing having length L_r,
(b) Housing twice as long as the rotor, with a span of $2L_r$, extending past both ends of the rotor, and
(c) Housing three times as long as the rotor, with a span of $3L_r$, extending past both ends of the rotor.

In all cases, the pump assembly was adequately modeled using: (1) Two constraint modes and three interior modes for the rotor,

and (2) Two constraint modes and two interior modes for the housing, in each of two orthogonal planes.

ROTORDYNAMIC PREDICTIONS WITH WATER

Base-Line Model. The assumed fluid properties with water are μ = 0.92cP; $\gamma = 62.31\frac{lb}{ft^3}$. The base-line model has new clearances and a housing model with length $2L_r$. The seal preswirl ratio (PSR) is defined as the inet circumferential velocity divided by the adjacent rotor surface velocity, PSR = $U_0/ R_s\omega$. Table 2 shows the assumed PSR values for the seals with and without swirl brakes.

Table 2. Preswirl Ratios

Seal	No swirl brakes	With wear ring swirl brakes
Front wear ring	0.7	0.1
Rear wear ring	0.7	0.1
Interstage	0.4	0.4
Impeller Insert	0.5	0.5

The 0.7 value assumed for the wear ring seals is commonly assumed for standard commercial pump impellers with tighter shroud clearances than those shown in Figures 6 and 7. One OEM representative has suggested that a lower value should be used based on their fluid velocity measurements in the front impeller-shroud space. The large clearances in the side wall spaces could support that view. However, the axial face seals upstream of the wear ring seals present a unique ESP feature. Depending on the axial clearance in the face seal, the circumferential leakage velocity exiting the face seals and entering the wear ring seals could approach $R_s\omega$ with the corresponding PSR =1 for the seals.

The interstage and impeller insert seals have assumed preswirl ratios of 0.4. This value assumes that the diffuser downstream of the impeller has reduced the circumferential velocity of the fluid approaching the interstage seal. Table A.1 in Appendix A contains the predicted rotordynamic coefficients at 3600 rpm. These coefficients produce a reaction force between the rotor and the housing that is proportional to the *relative* rotor-housing motion.

The base-line model is predicted to be stable out to running speeds in excess of 4000 rpm. A pump can be excited synchronously by mechanical imbalance, hydraulic imbalance, and bent-shaft excitation. The impellers are assumed to be mechanically balanced to an "API 4W/N" balance specification. Assuming that the stage ΔP is proportional to ω^2; i.e., $\Delta P = \alpha_P \omega^2$, then the impeller hydraulic imbalance magnitude is

$$F_{H\text{-}Imb} = 2\ \alpha_P\ K_{H\text{-}Imb}\ r_2\ b^*_2\ \omega^2 \qquad (6)$$

The lengths r_2 and b^*_2 are shown in Figure 13. For investment-cast impellers, Bolleter et al. [16] cite the following range for $K_{H\text{-}Imb}$.

$$.005 < K_{H\text{-}Imb} < .015$$

For this study, $K_{H\text{-}Imb}$ = .010, an average value between the two extremes.

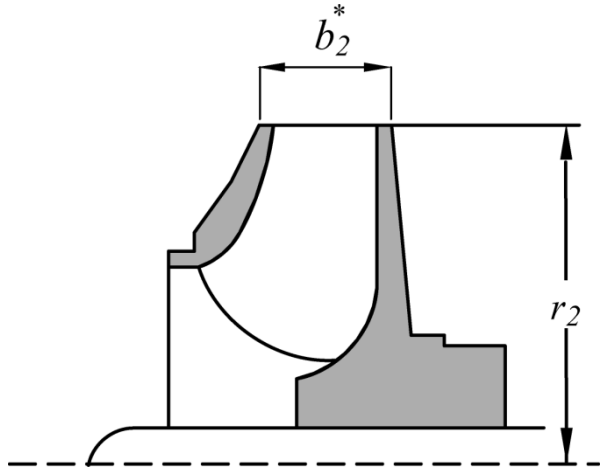

Figure 13. Impeller dimensions for hydraulic imbalance definition, Childs [4]

Bent-shaft excitation arises regularly in many rotating machines [17]. However, the straightening and assembly procedures used for ESPs can result in significant bent shaft excitation. A "representative" bent-shaft shape is used here with bent-shaft (displacement) shapes in the *x*-*z* and *y*-*z*, orthogonal, rotor-fixed planes. A corresponding set of slopes can be obtained from these bent-shaft deflections. Multiplying the bent-shaft shape in the respective planes by the rotor's free-free stiffness matrix will produce a set of rotor-fixed force and moment vectors that act on the right-hand side of the model as synchronous excitation vectors. They are similar to mechanical and hydraulic imbalance vectors but are constant and independent of running speed.

Figure 14 shows the predicted synchronous response amplitudes due to: (1) mechanical imbalance, (2) hydraulic imbalance, (3) bent-shaft excitation. The predictions in Figure 14A show *relative* rotor-housing response in the axial center of the pump rotor. The relative rotor-to-housing response synchronous amplitude resulting from mechanical and hydraulic imbalance is small compared to the minimum clearances of 5 mils. The major conclusions from Figure 14A are: (1) The amplitudes due to mechanical and hydraulic imbalance are comparable, and (2) The response amplitude due to bent-shaft excitation is much larger and is the major contributor to the total response.

Figure 14B presents the predicted housing-velocity amplitude at the axial center of the pump. Forsberg's [13] measured peak acceleration levels were 0.29g's at 3600 rpm, leading to a predicted peak velocity amplitude of 0.30 inches/sec. *Hence, without any direct collaboration, the present model predicts a housing response amplitude that is comparable to Forsberg's measured results.* The predicted velocity levels are clearly excessive in comparison to accepted standards for conventional pumps.

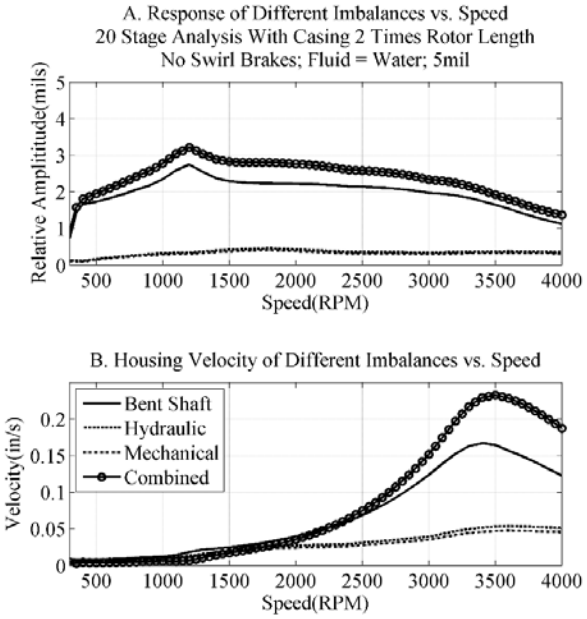

Figure 14. Predicted synchronous response due to mechanical imbalance, hydraulic imbalance, and bent-shaft excitation for the base-line ESP model with water. A. Mid-rotor response amplitude (mils). B. Housing velocity amplitude (inches/sec)

Figure 15 shows Forsberg's measured housing mode shape for the *full assembly* at 3600 rpm. Note that the data in this figure have been reduced to synchronous-response only, and any sub or supersynchronous motion has been removed. Figure 16 shows a rough orbit plotted from Figure 15. It is hour-glass shaped versus circular. Figure 17 shows the predicted mode shape for the *pump* model used here, reflecting a third-housing-mode shape for the reduced model. Given that Figure 15 shows a measured result for the full assembly, and Figure 17 shows predicted response for the pump housing only, one could argue that a comparison of the two figures represents "apples-and-oranges." However, even with the model reduction for the pump versus the full assembly, the measurements and predictions are clearly comparable. *One immediate conclusion from these plots is that a full-assembly model for ESPs is desirable, assuming that data are available to support its construction.*

Returning to Figures 14A-B, the maximum housing amplitude at 3600 rpm is near a housing resonance. Forsberg only presents data at one speed; hence, his pump may or may not have also been operating near a housing resonance. *Run-down water-fall plots from Forsberg's tests would have been very helpful in making more direct comparisons.*

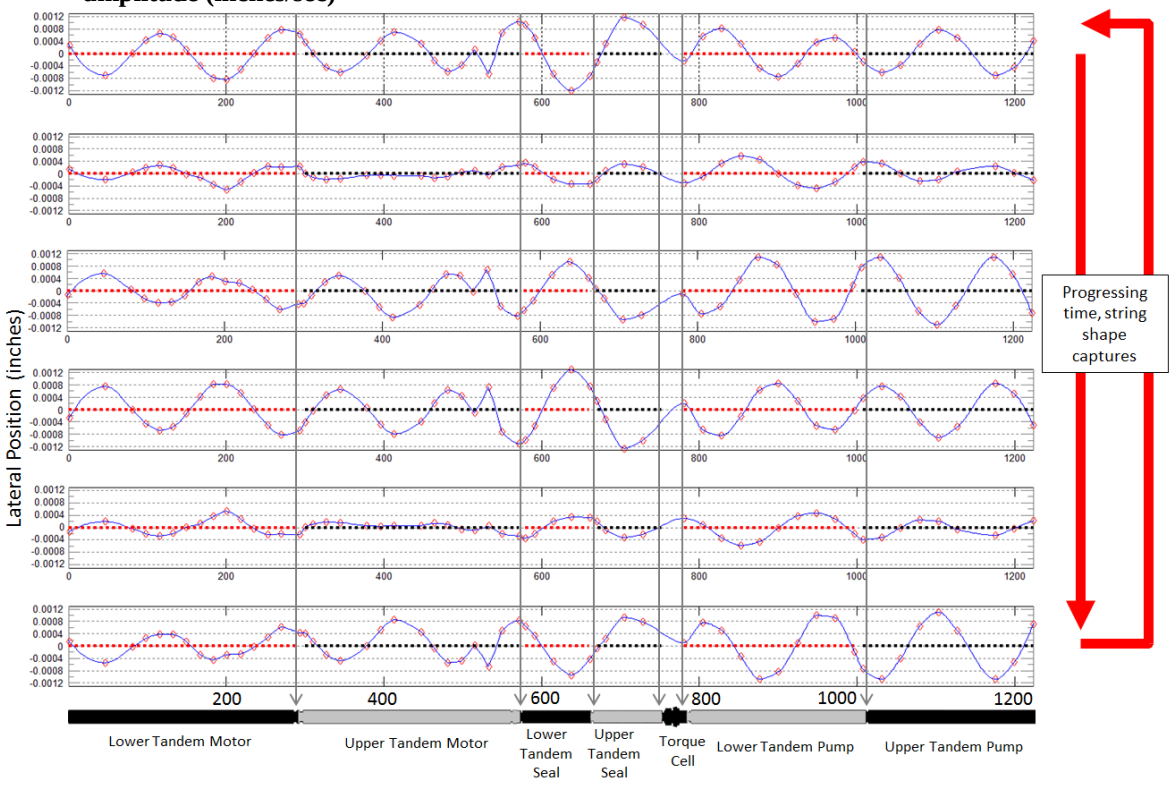

Figure 15 Forsberg's measured housing *assembly* response (from accelerometer output) at 3600 rpm [13]

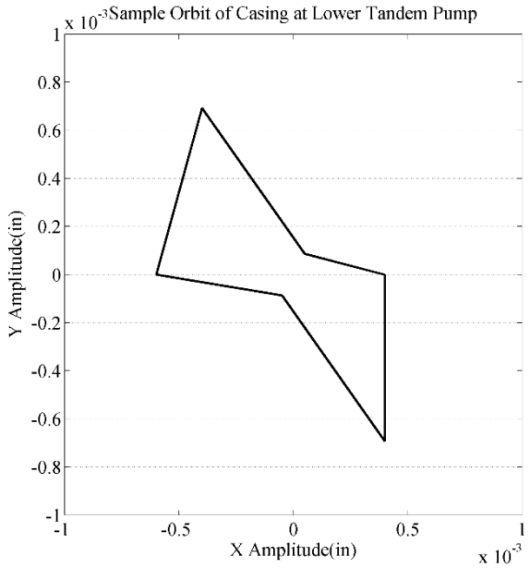

Figure 16. Constructed orbit from Forsberg's measured housing *assembly* response at 3600 rpm

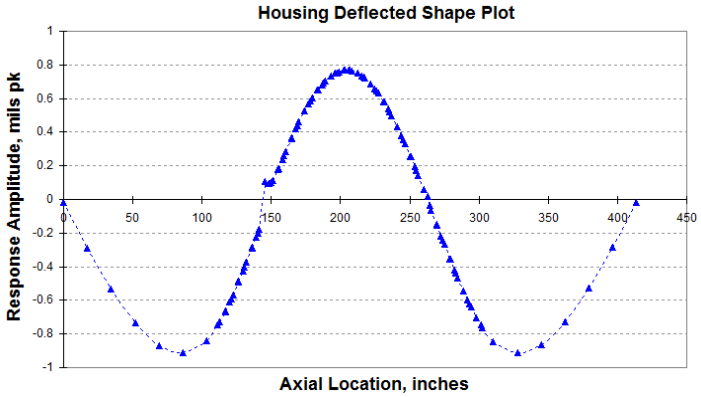

Figure 17. Predicted *pump* housing response amplitude at 3600 rpm

The Impact of Wear on Rotor Response and Stability with and without Effective Swirl Brakes

The calculations presented thus far are for new clearances. In this section, we consider the impact of increasing clearances due to wear. Figure 18 shows the real parts of some of the model's eigenvalues for doubled clearances with a change from positive to negative around 2300 rpm. Doubled clearances drop all of the rotordynamic coefficients, but particularly the direct damping and stiffness. Hence, the natural frequencies of rotor-casing modes drop, and their associated damping also drops. Table 3 shows the predicted onset speeds of instability (OSI) for the base-line pump model with new, doubled, and tripled clearances. Note the abrupt drop in the OSI due to increasing clearances.

Assuming that the wear ring seals had effective swirl brakes, *that would drop the wear ring seals' pre-swirl ratio to 0.1* (Table 2), Table 3 shows that the predicted OSI continues to lie well above the running speed of 3600 rpm even with 2X and 3X clearances.

One major lesson from Massey [9] and Valantas and Bolleter [10] concerning unstable pumps is that progressive failures ensue. Unstable motion with large amplitudes causes seal rubbing, which causes enlarged clearances, etc. The seals in Massey's pump were handling a clean hydrocarbon and wore out such that the pump had to be taken off line in 48 hours. Similar progressively increasing vibration levels following the initiation of unstable motion probably holds for ESPs. A combination of switching from grooved seals to smooth seals plus swirl brakes eliminated the instabilities in both these case studies [9-10]. *If applied to ESPs, operating with low viscosity fluids, swirl brakes could certainly stave off instabilities and significantly extend operating lifetimes.*

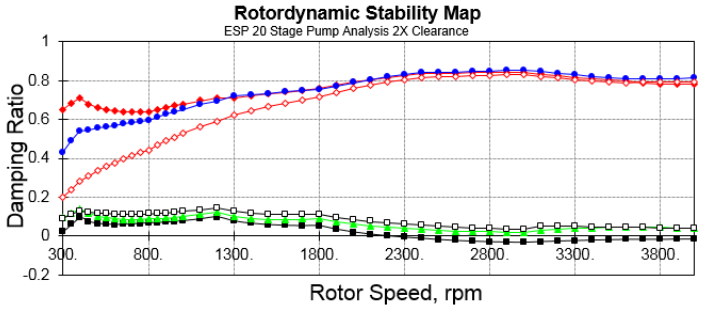

Figure 18. Damping ratio versus running speed for the first five rotor-housing modes. Base-line model with doubled clearances without swirl brakes.

Table 3. Predicted pump OSI with water for new, doubled, and tripled seal clearances.

Configuration	Original (RPM)	2X Clearance (RPM)	3X Clearance (RPM)
Without Swirl Brake	>4000	2200	850
With Swirl Brake	>4000	>4000	>4000

Note: The present stability analyses do not consider potential destabilizing forces and/or moments arising at the spline couplings. Cases have been cited in the past where various authors have cited spline couplings as the possible source of rotordynamic instabilities [5].

Synchronous Response with Water, Tripled Clearances, and Effective Swirl Brakes

Figure 19A shows the predicted relative rotor-housing response at pump mid-span using water for: (1) original clearances with and without swirl brakes, (2) doubled clearances with swirl brakes, and (3) tripled clearances with swirl brakes. The figure supports the following conclusions:

(1) At 3600 rpm, swirl brakes would reduce the response with the original clearances.
(2) Seal wear-out will steadily increase the peak response amplitudes.
(3) The response amplitudes start at 60% of the radial clearances and drop to a smaller fraction of clearances as the clearances increase.

Figure 19B shows the predicted housing vibration levels for the same arrangement of seal clearances and swirl brakes, supporting the following conclusions:

(1) Effective swirl brakes would modestly decrease housing vibration levels with the new clearances.

(2) Worn clearances markedly drop the housing vibration levels. The figure suggests that the coupled-rotor-housing mode natural frequency near 3600 rpm for new clearances has dropped markedly as the clearances increase.

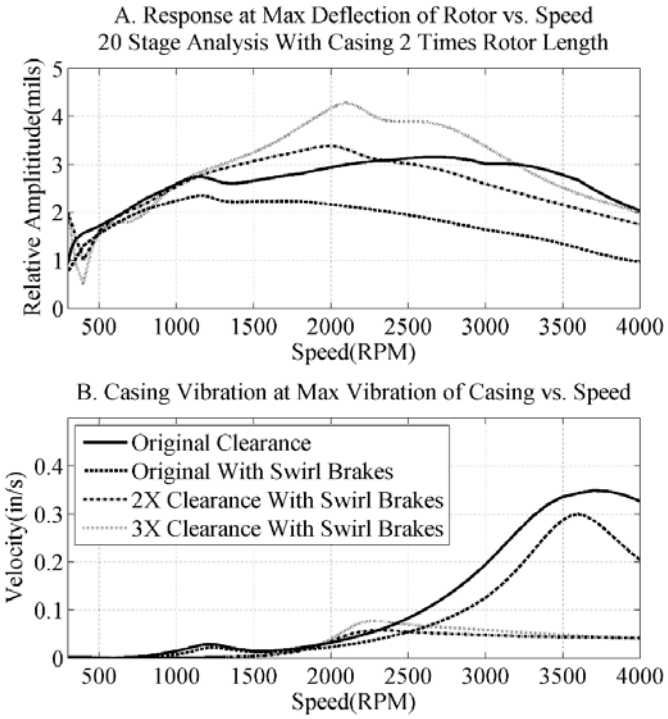

Figure 19. The impact on predicted synchronous response due to changing the seal clearances. A. Relative rotor-housing amplitudes, B. Housing vibration levels

The Impact of changing the Housing Boundary-Termination Locations

As noted above, when modeling the pump alone (versus a full-assembly model), questions arise regarding the impact of changing housing-termination locations. Figure 20 shows predicted relative rotor-housing responses and housing-velocity-response amplitudes for the following housing termination lengths: Housing that is 1.5, 2, and 3 times the rotor length. For all cases, the housing ends are pinned to ground. Figure 20A shows that the predicted relative rotor-housing response is largely unchanged by changing the termination location. By contrast, Figure 20B shows that the predicted housing-response-vibration levels change markedly with changes in the housing-termination location. The housing resonance frequency is above running speed for a 1.5X length termination, close to running speed for the 2X length termination, and around 3000 rpm for the 3X termination locations.

A major lesson (*again*) *from this plot is that the full assembly* (*versus a pump section*) *should be modeled to predict the housing's vibration behavior.* However, the predicted relative motion of the rotor and housing is largely insensitive to the housing termination location.

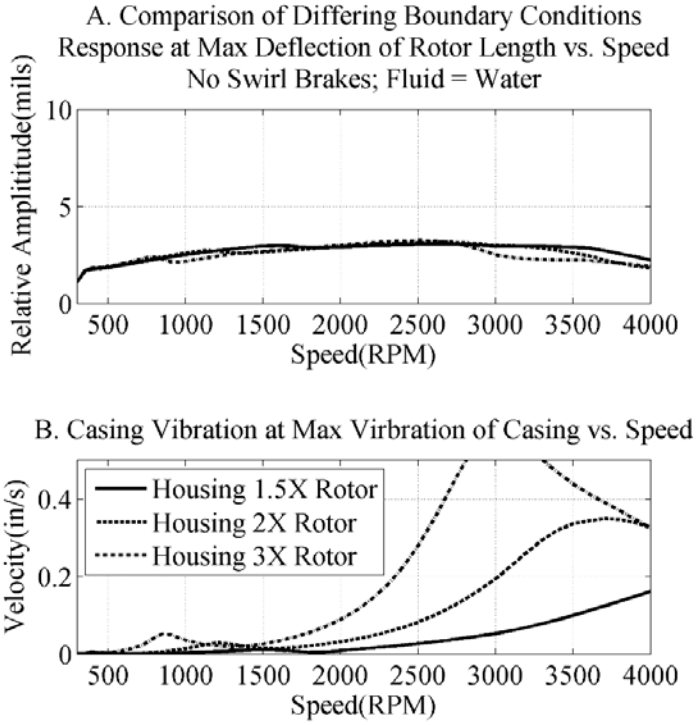

Figure 20. Impact of changing the housing-termination location for new clearances on: A. predicted relative rotor-housing motion, and B. Housing vibration amplitudes

Impact of Contact between the Pump Housing and the Column Piping

One issue that arises in modeling an ESP is the distinct possibility that the pump housing may contact the column piping. Obviously, there are an infinite number of possible contact scenarios. As a first step, we investigated the possibility of a single-point radial contact at the center of the pump that would provide major stiffening of the housing in one radial direction. A connecting spring with the radial stiffness coefficient $k_{contact}$ = 1.0 E+6 lb/in was used to connect the housing to ground in the X direction. For the original pump configuration, the OSI was above 8000 rpm without the pump housing-to-column connection, and it remains well above 8000 rpm with the housing-to-ground connection.

Figure 21 shows the predicted response for the base-line pump with a stiff elastic connection to ground from mid-span of the housing for 1X, 2X, and 3X clearances. In this case, the housing length is two times the pump length. Figure 21A shows little impact on the relative rotor-housing response. Figure 21B shows the housing velocity amplitude in the X (connection) direction. A dramatic drop in rotor-housing response amplitudes is predicted, presumably because the housing resonance has been pushed higher --- well beyond 4000 rpm. The predicted response is insensitive to changes in clearance. Figure 21C shows the predicted housing-velocity amplitude response in the Y direction (transverse to the connection direction). The connection is predicted to increase the amplitude with new clearances.

However, at 2X clearances, the amplitude drops, and at 3X clearances it increases (compared to 2X clearance predictions).

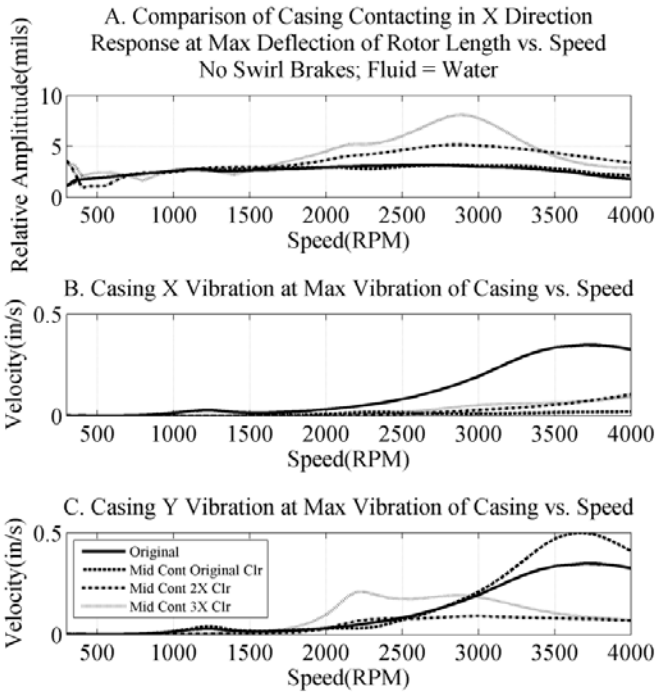

Figure 21. Predicted impact of a stiff elastic connection from mid-span of the pump housing to mid-span of the casing. A. Relative rotor housing response orbit amplitudes. B. Housing velocity amplitudes in the X (connection) direction. C. Housing velocity amplitudes in the Y (transverse-to-connection) direction.

Figure 22 shows predicted orbits of the housing (Figure 22A) and relative rotor-housing orbits (Figure 22B) at a mid-span location. The lateral connection in the X direction makes a major impact on the predicted housing response and a minimal impact on the relative rotor-housing orbit.

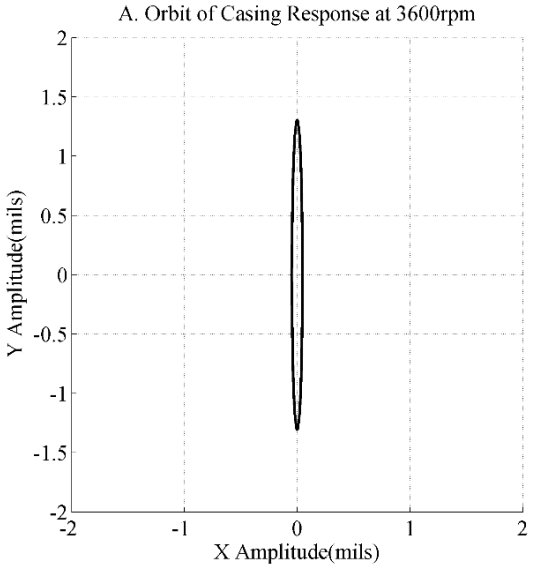

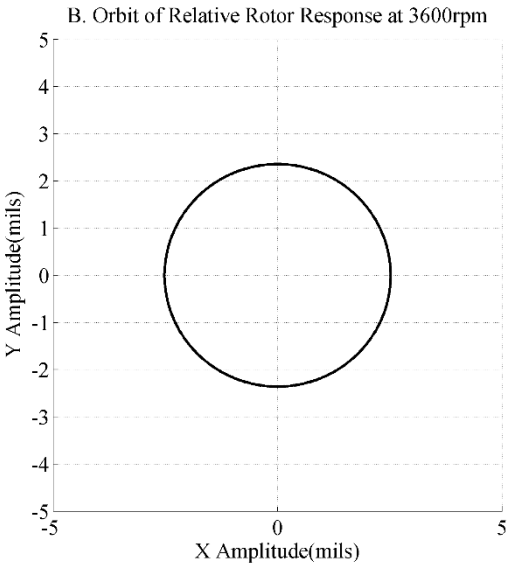

Figure 22. Predicted impact of contact between the pump housing and column pipe at housing mid-span for the base-line configuration: A. Mid-span housing orbit, and B. Mid-span relative rotor-housing orbit

ROTORDYNAMIC PREDICTIONS WITH AN OIL-WATER EMULSION

The water-oil emulsion is modeled for a fluid with the following physical properties: μ = 30cP; $\gamma = 53.66\frac{lb}{ft^3}$. The models for the pump using water and an emulsion have the same structural-dynamic model except for changes to added mass terms due to the density changes of the fluid contained in the impellers. The seal ΔPs also change because of the reduced density values.

For the emulsion-viscosity properties, at tight clearances, the reaction forces of the seals are developed more due to fluid rotation and act more like an uncavitated plain journal bearing than a Lomakin seal. The appropriate model for the seals/bushings is Eq. (5) with the rotordynamic coefficients strongly a function of the static eccentricity ratio. In a centered position, the predicted whirl frequency ratio (defined as the cross coupled stiffness coefficient, *Kxy*, divided by *C*ω, the direct damping coefficient multiplied by the shaft running speed, WFR = *Kxy/C*ω) for this model is 0.5, which is indicative of oil whirl. For eccentric seals, Lund's whirl-frequency definition is used [18].

The Impact of Static Eccentricity Offsets on Stability

The seals have negligible centering capabilities in the centered position. Without swirl brakes, an OSI of less than 300 rpm is predicted for the pump with centered seals. Conventional wisdom is that unstable vertical pumps can be stabilized by offsetting seals/bushings so that they operate at higher eccentricity ratios. To consider the impact of offsetting seals, we are going to assume that, in moving along the pump model from left to right, the first stage is offset in the +X direction, and the next seal is offset in the –X direction, etc., for all seals; hence, the seals are all loaded against each other. (Actually, the model

would give the same answers if all seals were displaced together along the same axis.) Table 1 shows that the interstage seals have the tightest clearance, and we are going to show the impact of changing their static eccentricity ratios on stability with corresponding but smaller eccentricity-ratio reductions for the other seals.

Table 4 presents predicted OSI versus interstage eccentricity ε_0 values for new clearances. Displacing the seals is predicted to rapidly elevate the OSI. ESP assembly procedures create unintentional stage offsets, and the predictions of Table 4 indicate that the unintended offsets could create a stable pump with new clearances.

Table 4. First damped natural frequency and OSIs versus interstage-seal offset eccentricity ratio ε0 for new clearances and no swirl brakes

Interstage seal ε_0	First ω_{d1} at 3600RPM (RPM)	OSI (RPM)
0.0	1762	<300
0.1	1788	2100
0.2	1822	6300
0.4	1970	>7000

Unlike conventional pumps, an ESP rotor starts in an unsupported state. The increasing speed and ΔP create supporting forces at seals that cause the multitude of rotor-housing modes to change and the natural frequencies to increase. The center column in Table 4 shows the damped natural frequency of the rotor-housing mode ω_{d1} that becomes unstable. Note that when the seals are centered ($\varepsilon_0 = 0$), ω_{d1} = 1762 rpm, a little less than one half of running speed at 3600 rpm. The increasing ε_0 offsets quickly push ω_{d1} to a higher value, also elevating the OSI level.

With an emulsion, and no swirl brakes, Figure 23 shows the impact of increasing clearances on the stability for eccentric seal positions. For new clearances, the OSI increases briskly with increasing ε_0 offsets values; however, increasing the clearance by 2X means that ε_0 offsets needs to be increased greatly to maintain stability. At 3X clearances, increasing ε_0 offsets is no longer effective.

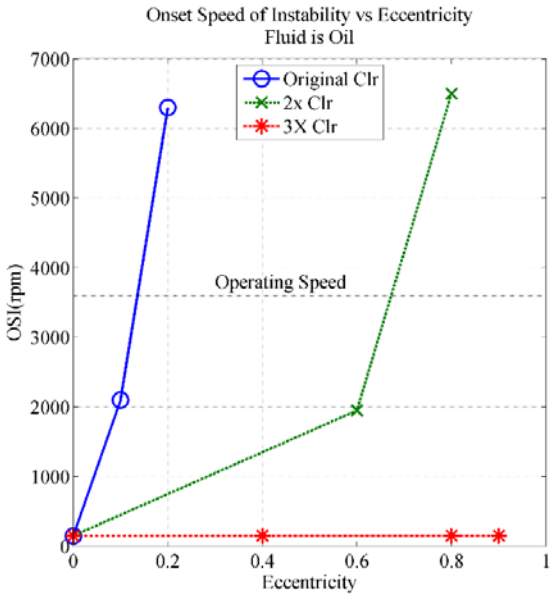

Figure 23. OSI versus ε_0, 1X, 2X, and 3X clearances

Figure 24 shows predicted relative rotor-housing response amplitudes and housing velocity response amplitudes for new clearances with the interstage seal eccentricity ratios: ε_0 = 0.2 and 0.4. The peak housing response resonance remains around 3600 rpm. However, the relative rotor-housing motion is greatly suppressed at all speeds.

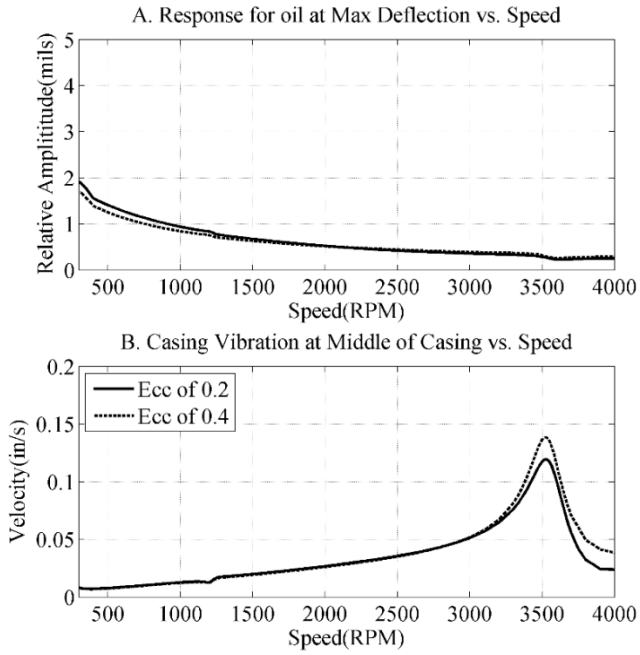

Figure 24. The impact on predicted synchronous response due to changing the seal static eccentricity ratios; new clearances, water-oil emulsion. A. Relative rotor-housing amplitudes, B. Housing vibration levels

The Impact of Swirl Brakes on Stability with Emulsions and Worn Clearances

As noted above, the reaction forces developed by annular seals arise due to both fluid rotation (as with plain journal bearings) and the Lomakin effect due to pressure-driven flow. With emulsions and new clearances, fluid rotation dominates, and swirl brakes are ineffective. The predictions of Figure 25 apply for small motion about a centered position.

Figure 25A shows

$$K_{eff} = K + c\,\omega - M\,\omega^2 \qquad (7)$$

versus ω for new and worn seals. Swirl brakes have little impact on K_{eff} . Remember in looking at this figure that: (1) ΔP is proportional to ω^2, and (2) The centering force due to fluid rotation drops briskly with increasing clearances. Hence, as C_r increases, the Lomakin effect increases, and K_{eff} also increases. Increasing K_{eff} increases the rotor's natural frequencies, and accordingly enhances stability. This increase in K_{eff} would not continue indefinitely. Childs [5] shows that, for Lomakin seals, K normally drops with increasing C_r .

Figure 25B shows very little impact of swirl brakes on whirl frequency ratio for new clearances with WFR approximately equal to 0.5. Without swirl brakes, WFR increases modestly with increasing ω for 2X clearances, but increases rapidly for 3X clearances. With swirl brakes, WFR drops with increasing ω --- modestly for 2X clearances, and sharply for 3X clearances. Given that higher WFR values indicate an increased probability of instability, Figure 25B clearly predicts that swirl brakes will be an effective stabilizing component for a pump handling emulsions with 2X and 3X clearances. Together with Figure 23's predictions that static offsets are effective for new clearances (but not worn clearances), swirl brakes are clearly recommended for ESPs handling emulsions.

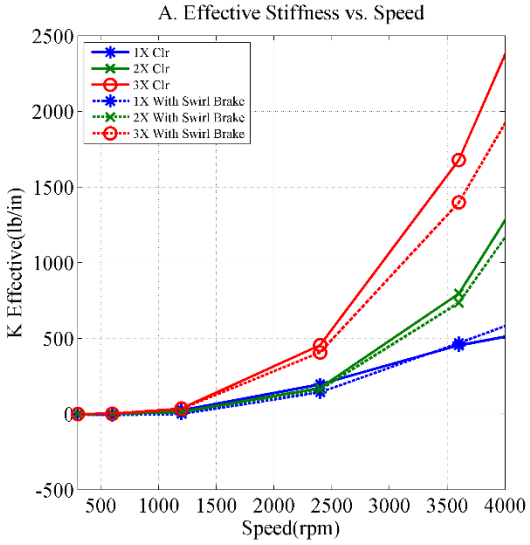

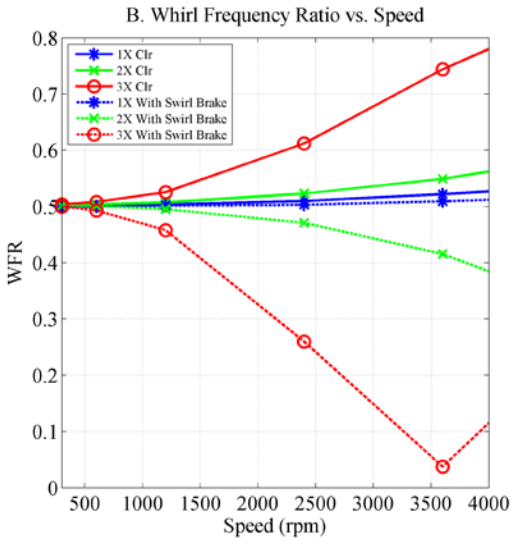

Figure 25. Emulsion predictions for 1X, 2X, and 3X clearances with and without swirl brakes; (A) K_{eff} versus ω, (B) WRF versus ω

The Rotordynamic Impact of a Contact Connection between the Pump Housing and the Well Casing with Emulsions

As with the cases above with the pump handling water, a spring with the radial stiffness coefficient $k_{contact}$ = 1.0 E+6 lb/in is used to attach the pump housing to the well casing at rotor mid-span. OSIs were predicted for the lateral connection with emulsions, and the connection had no appreciable impact on predicted stability.

Figure 26 shows the predicted response for the base-line pump with the eccentricity ratio ε_0 = 0.2.

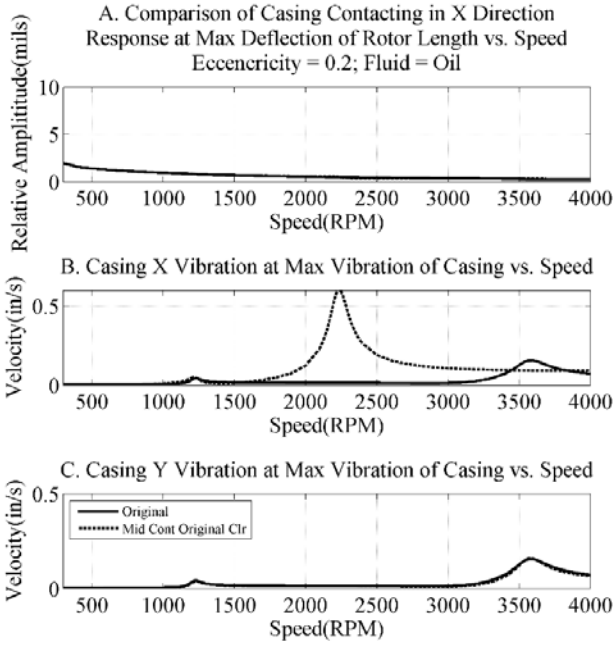

Figure 26. Response with and without housing-casing contact, new clearances, ε_0 = 0.2

Accounting for Fluid between the Housing and Column Piping

The previous predictions did not include the fluid between the housing OD and column ID. A recent reviewer asked about the impact of this fluid. The influence of a long non-rotating cylinder is listed by Black [20] as

$$\begin{bmatrix} -F_y \\ -F_z \end{bmatrix} = \begin{bmatrix} 2\bar{C} & 0 \\ 0 & 2\bar{C} \end{bmatrix} \begin{bmatrix} \dot{y} \\ \dot{z} \end{bmatrix} + \begin{bmatrix} m_a & 0 \\ 0 & m_a \end{bmatrix} \begin{bmatrix} \ddot{y} \\ \ddot{z} \end{bmatrix} \quad (8)$$

Where

$$\bar{C} = 6\pi\mu L \left(\frac{r}{Cr}\right)^3 \quad (9)$$

$$m_a = \rho\pi r^2 L \left(\frac{r}{Cr}\right) \quad (10)$$

Blevins [21] gives an alternate added-mass result for a cylinder in an infinite body of fluid; namely, the added mass is the volume of the cylinder times the density of the surrounding fluid. A comparison of these two model's added mass is provided in Figure 27. Blevins provides a prediction for added-mass only, no damping.

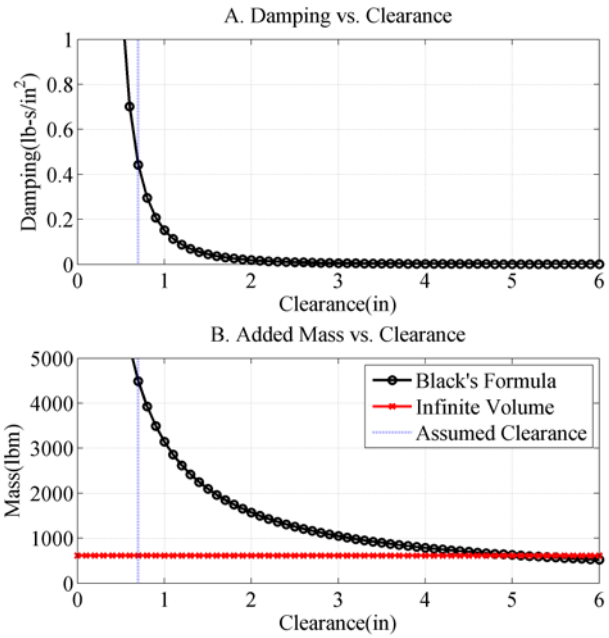

Figure 27. Predictions of the damping and added-mass for the fluid between the pump housing and well bore. A. Black's damping coefficient, B. Black's and Blevins's added-mass coefficient

Black's formula includes a 1/Cr factor in both the damping and added mass; hence, Black's damping and added mass terms vanish for an infinite volume in contrast to Blevins's model. For the small clearances considered here, Black's model is appropriate.

The radial clearance used in this analysis is 0.7in. This value was chosen as the median of several suggestions. The amount of added mass is the biggest change from accounting for the effects of the fluid. With a clearance of 0.7in the total pump added weight is approximately 4500lb which is close to three times the rotor weight. With an oil-water emulsion the added weight is reduced to 3800lb. The pump's added damping when the fluid cavity is the viscosity of water is relatively small at $0.4419\frac{lb*s}{in}$. For oil viscosity, the damping increases dramatically to $13.25\frac{lb*s}{in}$. The added mass and damping were distributed evenly across the length of the housing.

As shown in Figure 28, with water and new clearances, accounting for the fluid around the housing can be important for modeling an ESP's *housing* response. The casing resonance-peak frequencies dropped to around half their original values. This introduced three housing modes within the operating range instead of two. The relative rotor-housing response was only modestly affected. The OSI dropped from greater than 4000 rpm to only slightly above 3600 rpm.

With the same pump submerged in oil there are similar trends as in Figure 28. The housing natural frequencies of dropped to around half their original values. The relative rotor-housing response stayed the same. The major difference between enclosed water and oil is that the predicted OSI stayed the same (quite low) with or without the fluid added mass.

Forsberg' test results (figure 15) were obtained for large clearances around the test assembly for which the impact of water surrounding the assembly are predicted to be negligible. Hence, the good agreement between measurement and predictions cited for figures 14 and 17 remain valid.

Overall, if housing velocity or rotor stability is of concern the fluid between the housing OD and column ID should be included in the model.

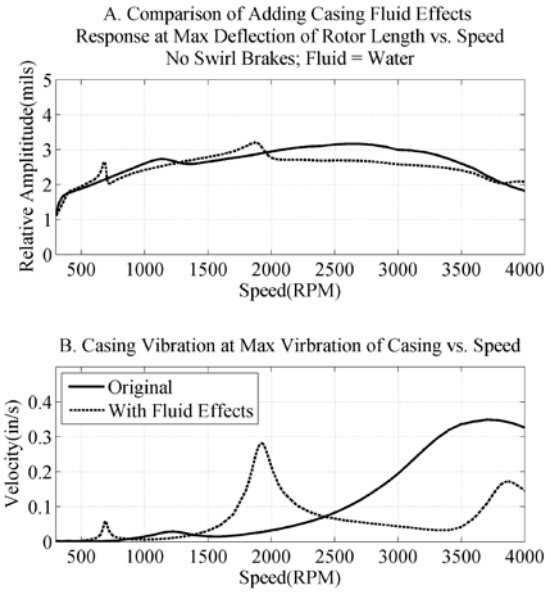

Figure 28. Effect of including the fluid interaction of the housing to column cavity on the A. relative response versus speed and B. housing vibration versus speed

SUMMARY, CONCLUSIONS, AND ISSUES

Stability and synchronous-response predictions are presented from a rotordynamic analysis for a *pump segment* of an Electrical Submersible Pump (ESP) assembly.

Rotordynamic properties of ESPs depend heavily on the internal reaction forces developed by annular seals. A *known* uncertainty considering ESP rotordynamics is the flow through the axial seals in Figures 7 and 8. The leakage flowing radially inwards through the axial face seals will be pre-rotated in the direction of shaft rotation due to the rotating seal face, and destabilizing forces are directly proportional to the fluid pre-rotation. The degree of pre-rotation depends on the axial clearance, fluid viscosity, and the leakage rate (which also depends on the axial clearance). The assumed pre-swirl ratios used in this study are based on experience with conventional pumps.

Synchronous-response predictions are presented for: (1) relative rotor-housing motion, and (2) housing-velocity-response amplitudes. Synchronous response is excited by: (1) mechanical imbalance (4W/N API balance spec), (2) hydraulic imbalance (at a midrange of expected levels for investment-cast impellers), and (3) bent-shaft excitation (based on representative data from direct bent-shaft eccentricity measurements). The predicted response amplitude contributions were comparable for the hydraulic and mechanical imbalances but much larger due to bent-shaft excitation.

When handling water, the rotor was predicted to be stable at new and centered (1X) clearances but rapidly became unstable with enlarged clearances (2X, 3X). The impact of introducing effective swirl brakes on stability and synchronous response was investigated for the wear ring seals showing: (1) Predicted instabilities were eliminated at all clearances out to greater than 8000 rpm, and (2) Synchronous response amplitudes were reduced modestly.

Housing-response amplitudes varied considerably with the choice of housing-termination locations. For a pump handling water, rotor length of L_r with a axially pump-centered housing of lengths ($1.5L_r$, $2L_r$, and $3L_r$), a sharp resonance peak moves across the running speed of 3600 rpm and produces vibration levels in excess of 0.5 inches/second. These predicted levels exceed most vibration codes; however, relative rotor-housing-response amplitudes were a small fraction of clearances for all cases. Similar, but reduced changes in response were predicted for ESPs handling high-viscosity emulsions.

When handling emulsions with elevated viscosity levels, the rotor was unstable for seals with new 1X clearances at a centered position (OSI<300 rpm). The predicted OSI rapidly increased as the seal stators were displaced eccentrically, moving well above running speed. With the seals displaced eccentrically and the pump predicted to be stable, the synchronous relative rotor-housing motion was a small fraction of seal clearances. The housing motion continued to show a sharp peak near running speed with a predicted velocity amplitude of 0.125 inches/second.

An ESP housing can contact the well casing in a range of possible scenarios (contact locations, length or girth of contact, etc.). As a starting point for analysis, a mid-span, point, radial contact was examined and modeled via a stiff housing-casing spring connection. For water and oil-water emulsions, the contact produced major elliptical housing motion. However, it had a comparably minor impact on relative rotor-housing response amplitudes or stability.

Based on horizontal, surface applications of ESPs, Durham in 1990 stated that most ESP failures were caused by mechanical-seal failures, and the mechanical-seal failures were caused by vibrations. The pump sections of the assemblies were not failing due to rubbing contact; the mechanical seals were failing. The first lesson from Durham is that a model for the *full* assembly (including the motor and seal sections shown in Figure (5) is needed to: (1) Examine the stability properties for the full assembly (specifically including the motor and its bearings), and (2) Examine the vibration levels at mechanical seal locations on the full assembly.

In 2005, based on direct measurements for a range of vertical and horizontal pumps, Stefanko and Lieshear [19] developed an empirical relationship between lateral vibration levels between mechanical seal lifetimes and lateral vibration levels. Their work was done at the Savanah River nuclear facility and directly supports Durham's prior work on ESPs; namely, *lateral vibrations kill mechanical seals leading directly to pump failures*.

To the extent that *pump* rotordynamic problems cause mechanical-seal failures, rotordynamic instabilities appear to be a greater hazard than synchronous-response amplitudes, because observed subsynchronous motion in conventional pumps can be much larger than synchronous vibration levels.

In terms of synchronous vibration levels, Forsberg's measured response curve in figure 15 shows marked changes in vibration amplitudes associated with only modest changes in axial position. Hence, a mechanical seal might experience high vibrations and a short lifetime at one axial location and have low vibrations and a long lifetime at a nearby location.

Briefly, other lessons are:

1. A straightforward rotordynamic model for an ESP produces predictions that agree reasonably well with the limited existing test data.
2. Instabilities for ESPs handling low-viscosity fluids can be prevented by using conventional swirl brakes, even with greatly worn clearances
3. With new 1X clearances, predicted onset speed of instabilities for ESPs that are handling high-viscosity fluids can be markedly elevated above running speed by offsetting the seals at comparatively low static eccentric ratios. The effectiveness of static offsets for stability-enhancement drops rapidly at 2X clearances, and vanishes for 3X clearances.
4. For pumps handling emulsions, swirl brakes become increasingly effective in elevating pump OSIs as the clearances increase and the seals begin to operate more like a Lomakin seal and less like a plain journal bearing.

Predictions of this study support the following views and recommendations: (1) Applying swirl brakes to ESP wearing-ring seals can significantly increase ESP lifetimes, (2) Models and analysis of a full ESP assembly are needed to directly examine options for reducing vibrations levels at mechanical

seals, thereby extending ESP lifetimes, and (3) Analyses, models, and tests are needed to quantify Durham's views regarding the failure of mechanical seals due to lateral vibrations.

Most of this study was conducted neglecting the influence of the fluid between the pump-housing OD and the column pipe ID. At the request of a reviewer, late (and brief) calculations were performed accounting for the added mass and damping due to this fluid. Accounting for these terms had a notable impact on predicted housing response, but a secondary impact on relative rotor-housing response and system stability. Future work will more thoroughly investigate the impact of this enclosed fluid.

NOMENCLATURE

C_r	Centered radial clearance	[L]
C_r/R	Clearance-to-radius ratio	[-]
D	Seal or bearing shaft diameter	[L]
e_0	Static displacement of a bearing journal due to an applied load	[L]
L	Seal or bearing length	[L]
L/D	Seal length-to-diameter ratio	[-]
PSR=$U_0/R_s\omega$	Preswirl ratio	[-]
R	Shaft radius	[L]
U	Fluid average circumferential velocity	[L/T]
$u=U/R\omega$	Nondimensional fluid circumferential velocity	[-]
W	Fluid bulk-flow axial velocity	[L/T]
$\varepsilon_0= e_0/C_r$	Static eccentricity ratio	[-]
μ	Lubricant viscosity	[F-T/L^2]
γ	Lubricant specific weight	[F/L^3]
ω	Shaft running speed	[T^{-1}]
WFR=$k/C\omega$	Whirl Frequency ratio for a centered seal	[-]

APPENDIX A

Table A.1. Seal operating at 3600 rpm with water *in a centered position* (ΔP, Flow rate, K, k, C, c, M, WFR)

Original Clearance Seal Properties at 3600rpm								
Seal	ΔP(psi)	Flow rate (lb/s)	K(lb/in)	k(lb/in)	C($\frac{lb*s}{in}$)	c($\frac{lb*s}{in}$)	M($\frac{lb*s^2}{in}$)	WFR
Front Wear Ring	24.50	1.60	2100	3520	10.5	1.9	0.0048	0.892
Rear Wear Ring	24.50	2.96	2010	2330	8.0	1.9	0.0048	0.775
Impeller Insert	1.30	0.37	9	43	0.3	0.1	0.0003	0.436
Interstage	33.70	0.32	3712	2220	16.3	5.0	0.0126	0.360

Double Clearance Seal Properties at 3600rpm								
Seal	ΔP(psi)	Flow rate (lb/s)	K(lb/in)	k(lb/in)	C($\frac{lb*s}{in}$)	c($\frac{lb*s}{in}$)	M($\frac{lb*s^2}{in}$)	WFR
Front Wear Ring	24.50	4.36	1709	1798	6.0	1.0	0.0024	0.791
Rear Wear Ring	24.50	7.47	902	1417	4.7	0.8	0.0020	0.798
Impeller Insert	1.10	0.84	5	20	0.1	0.0	0.0001	0.392
Interstage	33.90	0.88	1068	1279	8.5	2.6	0.0078	0.397

Triple Clearance Seal Properties at 3600rpm								
Seal	ΔP(psi)	Flow rate (lb/s)	K(lb/in)	k(lb/in)	C($\frac{lb*s}{in}$)	c($\frac{lb*s}{in}$)	M($\frac{lb*s^2}{in}$)	WFR
Front Wear Ring	24.50	7.38	1026	1340	4.5	0.5	0.0014	0.793
Rear Wear Ring	24.50	12.16	495	1028	3.5	0.4	0.0011	0.788
Impeller Insert	1.47	1.60	4	18	0.1	0.0	0.0001	0.407
Interstage	33.53	1.58	729	794	5.5	1.7	0.0052	0.381

Table A.2. Seal operating at 3600 rpm with an oil emulsion, new centered clearances

Oil Seal Properties at 3600rpm			
Seal	ΔP(psi)	Flow rate (lb/s)	WFR
Front Wear Ring	24.50	0.18	0.500
Rear Wear Ring	24.50	0.50	0.500
Impeller Insert	0.47	0.01	0.500
Interstage	34.53	0.01	0.500

REFERENCES

[1] Scarsdale, Kevin (2012), Panel Session, ESP Qualification and Reliability, Multiphase Pump User Roundtable (MPUR), Houston, TX

[2] Durham, M. (1990), "Effect of Vibration on Electric-Submersible Pump Failures," SPE Journal of Petroleum Technology, February, pp. 186-190.

[3] Corbo, M., Stefanko, D. and Leishear, R. (2002), "Practical Use of Rotordynamic Analysis To Correct a Vertical Long Shaft Pump's Whirl Problem," Proceedings, 19th International Pump Users Symposium, Houston, TX, pp. 107-120.

[4] Salas, K., Delgado, A., Van Dam, J., Marvel, R., and Sakamoto, S. (2013) "Rotordynamic Characterization of an Electric Submersible Pump Motor, " Society of Petroleum Engineers (SPE), ESP Workshop, Houston, TX

[5] Childs, D. (2013), Turbomachinery Rotordynamics with Case Studies, Minter Spring Publishing, ISBN# 978-0-615-85272-0

[6] Gunter, E.J., (1972), "Rotor-Bearing Stability," Proceedings, 1st Turbomachinery Symposium, College Station, TX, pp. 119-141.

[7] Leader, M. (2010), "Evaluating and Correcting Subsynchronous Vibration in Vertical Pumps," Case Study, The International Pump Users Symposium, 15-18 March 2010, Houston, Texas; organized by The Turbomachinery Laboratory, Texas A&M University

[8] Massey, I., (1985), "Subsynchronous Vibration Problems in High-Speed Multistage Centrifugal Pumps," Proceedings, 14th Turbomachinery Symposium, organized by Texas A&M University, pp. 11-16

[9] Valantas, R., and U. Bolleter (1988), "Solutions to Abrasive Wear-Related Rotordynamic Instability Problems in Prudhoe Bay Injection Pumps," Proceedings, 5th International Pump Users Symposium, organized by the Turbomachinery Laboratory at Texas A&M University, pp. 3-10

[10] Forsberg, M. (2013), "Evaluation of ESP Vibration: Technical Process versus Black Magic," Society of Petroleum Engineers (SPE), ESP Workshop, Houston, TX

[11] Bolleter, U., A. Wyss, I. Welte, and R. Stürchler (1987) "Measurement of Hydrodynamic Interaction Matrices of Boiler Feed Pump Impellers, ASME Trans. J. of Vibration, Stress, and Reliability in Design, 109 (**151**), pp. 144-151

[12] Rivera, R. (2013), Director, Kinetic Pump Innovations, LP, Houston, TX, Personal Communication

[13] Lomakin, A. (1958), "Calculation of Critical Number of Revolutions and the Conditions Necessary for Dynamic Stability of Rotors in High-Pressure Hydraulic Machines when Taking into Account Forces Originating in Sealings," Power and Mechanical Engineering, April 1958 (in Russian).

[14] Zirkelback, N., and San Andrés, L., 1996, "Bulk-Flow Model for the Transition to Turbulence Regime in Annular Seals," *STLE Tribology Transactions*, **39** (4), pp. 835-842.

[15] Semanate, J., and San Andrés, L., 1993, "Thermal Analysis of Locked Multi-Ring Oil Seals," Tribology International, **27**, pp. 197-206

[16] Bolleter, U., E. Liebungut, R. Stürchler, and T. McCloskey (1989) "Hydraulic Interaction and Excitation Forces of High Head Pump Impellers," Proceedings of Third Joint ASCE/ASME Pumping Machinery Symposium, San Diego, California, pp. 187-193

[17] Ehrich, F. (1992), Handbook of Rotordynamics, McGraw Hill, 1992

[18] Lund, J.W. (1966), "Self-Excited, Stationary Whirl Orbits of a Journal in a Sleeve Bearing," Ph.D. Thesis, Rensselaer Polytechnic Institute, Troy, NY

[19] Stefanko, D. and Leishear, R. (2005), "Relationship Between Vibrations and Mechanical Seal Failures on Centrifugal Pumps," Proceedings ASME International Mechanical Engineering Congress and Exposition, 5-11 November Orlando, Florida USA

[20] Black, H. (1979), "Effects of Fluid-Filled Clearance Spaces on Centrifugal Pump and Submerged Motor Vibrations," 8th Turbomachinery Symposium, Turbomachinery Laboratory, Texas A&M University, College Station, TX, pp. 29-34

[21] Blevins (2001), Formulas for Natural Frequency and Mode Shape, Krieger